

Article

# Non-Relativistic Treatment of the 2D Electron System Interacting via Varshni–Shukla Potential Using the Asymptotic Iteration Method

Collins Okon Edet <sup>1,2,3,\*</sup>, Salman Mahmoud <sup>4</sup>, Etido P. Inyang <sup>5</sup>, Norshamsuri Ali <sup>2,\*</sup>, Syed Alwee Aljunid <sup>2</sup>, Rosdisham Endut <sup>2</sup>, Akpan Ndem Ikot <sup>6</sup> and Muhammad Asjad <sup>7</sup><sup>1</sup> Faculty of Applied and Human Sciences, Universiti Malaysia Perlis, Kangar 01000, Malaysia<sup>2</sup> Faculty of Electronic Engineering Technology, Universiti Malaysia Perlis, Kangar 01000, Malaysia<sup>3</sup> Department of Physics, Cross River University of Technology, Calabar PMB 1123, Nigeria<sup>4</sup> Platform for Research and Analysis in Environmental Sciences (PRASE), Lebanese University, Beirut 1102, Lebanon<sup>5</sup> Department of Physics, National Open University of Nigeria, Jabi-Abuja PMB 581, Nigeria<sup>6</sup> Theoretical Physics Group, Department of Physics, University of Port Harcourt, East/West Road, Choba PMB 5323, Nigeria<sup>7</sup> Department of Mathematics, Khalifa University, Abu Dhabi 127788, United Arab Emirates

\* Correspondence: collinsokonedet@gmail.com (C.O.E.); norshamsuri@unimap.edu.my (N.A.)

**Abstract:** The nonrelativistic treatment of the Varshni–Shukla potential (V–SP) in the presence of magnetic and Aharanov–Bohm fields is carried out using the asymptotic iteration method (AIM). The energy equation and wave function are derived analytically. The energy levels are summed to obtain the partition function, which is employed to derive the expressions for the thermomagnetic properties of the V–SP. These properties are analyzed extensively using graphical representations. It is observed that in the various settings of the analysis, the system shows a diamagnetic characteristic, and the specific heat capacity behavior agrees with the recognized Dulong–Petit law, although some slight anomaly is observed. This irregular behavior could be attributed to a Schottky anomaly. Our findings will be valuable in a variety of fields of physics, including chemical, molecular and condensed matter physics, where our derived models could be applied to study other diatomic molecules and quantum dots, respectively.

**Keywords:** Schrödinger equation; Varshni–Shukla potential; magnetic field; Aharanov–Bohm field; topological defect

**MSC:** 81V17; 81V19; 81V55; 81Vxx; 82D99



**Citation:** Edet, C.O.; Mahmoud, S.; Inyang, E.P.; Ali, N.; Aljunid, S.A.; Endut, R.; Ikot, A.N.; Asjad, M. Non-Relativistic Treatment of the 2D Electron System Interacting via Varshni–Shukla Potential Using the Asymptotic Iteration Method. *Mathematics* **2022**, *10*, 2824. <https://doi.org/10.3390/math10152824>

Academic Editors: Panayiotis Vafeas and Yuri Shestopalov

Received: 23 May 2022

Accepted: 5 August 2022

Published: 8 August 2022

**Publisher's Note:** MDPI stays neutral with regard to jurisdictional claims in published maps and institutional affiliations.



**Copyright:** © 2022 by the authors. Licensee MDPI, Basel, Switzerland. This article is an open access article distributed under the terms and conditions of the Creative Commons Attribution (CC BY) license (<https://creativecommons.org/licenses/by/4.0/>).

## 1. Introduction

Topology plays a very important role in modifying the physical properties of diverse quantum systems. This concept is a crucial topic in research areas such as gravitation theory and condensed matter physics. The investigation of quantum systems in the presence of the impact of gravitational field has been a subject of profound interest for more than ten decades now [1]. Topological defects emerge in gravitation as monopoles, strings and walls [2–5]. Condensed matter physics presents these defects, such as vortices in superconductors or superfluids [2,6], domain walls in magnetic materials [7], solitons in quasi-one-dimensional polymers [4] and dislocations or disclinations in disordered solids or liquid crystals [5]. The alteration in the topology of a system presented by a linear defect such as a disclination in an elastic solid or a cosmic string in spacetime has strong effects on the physical properties of the medium [6,8]. In this area of research, the hydrogen atom, for example in curved spacetimes, has been considered [1]. When an atom is subjected to a

gravitational field, it is impacted by its interaction with the local curvature in addition to the topology of the spacetime [5].

In order to study how these defects affects quantum systems or related physical phenomena, potential models are usually adopted to depict such physical systems. In the numerous papers published extensively, the attention has been paid to exactly solvable models, particularly the harmonic oscillator, Cornell and Kratzer potentials whose nonrelativistic treatment is easily obtained [5,7]. Apart from an attempt by Nwabuzor et al. [9] and Edet and Ikot [10] to study multiparameter exponential-type models, the literature is still lacking in this direction. Hence, no study has been able to investigate the effects of these defects on molecules and quantum dots using exponential-type potentials. At the present time, not only have topological defects' effects on physical systems been probed, some effects related to the magnetic field, Rashba effect, Aharonov–Bohm field, Dresselhaus effects, etc. have also been studied. It has been pointed out that these fields also play very relevant roles in modifying the behavior of certain quantum systems [11–17]. Of note among these is the elimination of degeneracy by the magnetic field [18]. Moreover, of late, it has been found that the Aharonov–Bohm (AB) field plays such roles when introduced to a system [11,17,18]. Interestingly, some studies focusing on the effects of these perturbations have been presented by several authors [14,16,19–23]. Rampho et al. [24] studied in the presence of magnetic and AB fields the spectra of energy of diatomic molecules. Edet et al. [25] probed at finite temperature the magnetic susceptibility of Hellmann's potential and the properties of the heat AB flux and the field of magnetism. Karayer [26] analyzed the effects of the magnetic and AB fields on the energy spectra of the spatially varying mass interacting with the superposition of a Morse potential and a Coulomb potential. The effects of the AB and magnetic fields on the Shannon information entropy have been scrutinized by Edet and Ikot [27].

Following a well-established path by these studies, this study seeks to investigate the effects of perturbing external fields on the thermodynamic and magnetic properties of V–SP. It is therefore our goal in this paper to solve the 2D SE with perturbations with the Varshni–Shukla potential as an interaction potential using the asymptotic iteration method (AIM). The obtained energy is used to study the thermal and magnetic properties, considering the effects of the perturbations. This study is inspired by the fact that there exist possibilities of using the vibrational spectroscopy of diatomic molecules as an (approximate) probe for topological defects in the cosmos, although probes in this direction have been proposed earlier, for example, using Rydberg atoms [5], Lamb shifts [3,5] and shifts in energy of hydrogen atoms [1].

In view of this, this paper is organized in the following order. In Section 2, the solutions of the SE with the Varshni–Shukla potential are presented. The thermomagnetic and transport properties of the system are presented in Section 3. In Section 4, concluding remarks and a future outlook are presented.

## 2. Theory and Solutions

In this section, the model adopted for our study is discussed. Our choice of the Varshni–Shukla potential is motivated by the basic function it plays in modern physics [28–31]. This model has been employed to study scattering states in relativistic and nonrelativistic studies [28–30]. Some studies have also pointed out that this potential can describe the 2-body energy portion of multibody condensed matter [28]. Very recently, Inyang et al. [32] studied quarks with this model. The model under consideration is given as follows:  $V(r) = p - pqe^{-\delta r}/r$ , where  $p$  and  $q$  are adjustable potential parameters,  $\delta$  is the screening parameter and  $r$  the interparticle distance. Assuming there is a disclination or topological defect in this region, the disclination is explained using the line element  $ds^2 = dr^2 + \alpha^2 r^2 d\phi^2 + dz^2$  [6], where  $0 < \alpha < 1$  signifies the deficit of angle and has a relationship with the linear mass density  $\tilde{\mu}$  of the string using  $\alpha = 1 - 4\tilde{\mu}$  [3]. One can see that the azimuthal angle is expressed in the range  $0 \leq \phi \leq 2\pi$  [9]. For a particle charged and whose motion is limited to the region of the V–SP under the collective influence of the AB flux

and an external magnetic field with topological defect, the SWE for this case is defined in the following form [10]:

$$\left[ \frac{1}{2\mu} \left( i\hbar \vec{\nabla}_\alpha - \frac{e}{c} \vec{A}_\alpha \right)^2 + p - \frac{pqe^{-\delta r}}{r} \right] \Psi(r, \varphi) = E_{nm} \Psi(r, \varphi), \tag{1}$$

where  $E_{nm}$  signifies the energy level,  $\mu$  is the particle’s mass,  $\vec{A}_\alpha = \vec{B} \tilde{V}(r) \hat{\phi} / \alpha + \phi_{AB} / (2\pi r) \hat{\phi}$  is the vector potential with  $\tilde{V}(r) = e^{-\delta r} / (1 - e^{-\delta r})$ ,  $\vec{B}$  is the magnetic field and  $-AB$  represents the additional magnetic flux (AB effect) [33]. Here,  $\Psi(r, \varphi)$  is the wave function which can be written in cylindrical coordinates as  $\Psi(r, \varphi) = e^{im\varphi} R_{nm}(r) / \sqrt{2\pi r}$ , where  $m$  denotes the magnetic quantum number. Inserting this wave function and the vector potential into Equation (1), we arrive at the following radial second-order differential equation:

$$\frac{d^2 R_{nm}(r)}{dr^2} + \frac{2\mu}{\hbar^2} \{ E_{nm} - V_{eff}(r) \} R_{nm}(r) = 0, \tag{2}$$

where  $V_{eff}(r)$  is the effective potential and is given by

$$V_{eff}(r) = V(r) + \frac{\hbar\omega_c\beta_0\tilde{V}(r)}{r} + \frac{\mu\omega_c^2\tilde{V}^2(r)}{2} + \frac{\hbar^2\tilde{m}}{2\mu r^2}, \tag{3}$$

where  $\omega_c = e\vec{B}/(\mu c)$  is the cyclotron frequency,  $\beta_0 = m/\alpha^2 + \zeta/\alpha$  and  $\tilde{m} = (m/\alpha + \zeta)^2 - 1/4$  are integers with  $\zeta = \phi_{AB}/\phi_0$  and  $\phi_0 = hc/e$  is the flux’s quantum number. Equation (3) is not exactly solvable due to the presence of a centrifugal term. Therefore, we employ the Greene and Aldrich approximation [34] to overcome the centrifugal term. This approximation is given by  $1/r^2 = \delta^2 / (1 - e^{-\delta r})^2$ . We point out here that this approximation is only valid for small values of the screening parameter  $\eta$ . Therefore, by using the Greene and Aldrich approximation and introducing a new variable  $t = e^{-\delta r}$ , Equation (3) can be written as

$$\frac{d^2 R_{nm}(t)}{dt^2} + \frac{1}{t} \frac{dR_{nm}(t)}{dt} - \frac{P_0 t^2 - P_1 t + P_2}{t^2(1-t^2)} R_{nm}(t) = 0, \tag{4}$$

where  $P_0 = \epsilon_{nm} + \Lambda_0 + \Lambda_2$ ,  $P_2 = 2\epsilon_{nm} + \Lambda_0 - \Lambda_1$ ,  $P_1 = \epsilon_{nm} + \tilde{m}$  with  $\epsilon_{nm} = 2\mu(E_{nm} - a) / (\hbar^2 \eta^2)$ ,  $\Lambda_0 = 2\mu ab / (\hbar^2 \eta)$ ,  $\Lambda_1 = 2\mu\omega_c / (\hbar^2 \eta \tilde{\beta})$  and  $\Lambda_2 = \mu^2 \omega_c^2 / (\hbar^2 \eta^2)$ . In order to solve Equation (4), we have to transform differential Equation (4) into a form solvable by a standard mathematical technique. Hence, we take the radial wave function of the form  $R_{nm} = t^\vartheta (1-t)^g f_{nm}(t)$ , where  $g = \sqrt{\epsilon_{nm} + \tilde{m}}$  and  $\vartheta = \sqrt{\Lambda_1 + \Lambda_2 + \tilde{m} + 1/4} + 1/2$ . On substitution of the ansatz into Equation (4), we obtain the following hypergeometric differential equation:

$$\frac{d^2 f_{nm}(t)}{dt^2} - \lambda_0(t) \frac{df_{nm}(t)}{dt} - s_0(t) f_{nm}(t) = 0, \tag{5}$$

where  $\lambda_0(t) = [(2\vartheta + 2g + 1)t - (2\vartheta + 1)] / t(1-t)$  and  $s_0(t) = (\vartheta + g)^2 - (\epsilon_{nm} + \Lambda_0 + \Lambda_2) / t(1-t)$ . Equation (5) is a more suitable second-order homogeneous linear differential equation, the solution of which can be achieved by using the well-known asymptotic iteration method [10,35]. The asymptotic feature of the method for sufficiently large  $k$  is given as  $s_k(t) / \lambda_k(t) = s_{k-1}(t) / \lambda_{k-1}(t) = \gamma(t)$  with  $\lambda_k(t) = \lambda'_{k-1}(t) + s_{k-1}(t) + \lambda_0(t)\lambda_{k-1}(t)$  and  $s_k(t) = s'_{k-1}(t) + s_0(t)\lambda_{k-1}(t)$ . This, in principle, is referred to as the recurrence relation [35]. In accordance with the asymptotic iteration method [33,36], the equation we seek can be obtained from the roots of the following Equation [35]:

$$\delta_k = \begin{vmatrix} \lambda_k(t) & s_k(t) \\ \lambda_{k+1}(t) & s_{k+1}(t) \end{vmatrix} = 0, \text{ for } k = 0, 1, 2, \dots, n. \tag{6}$$

By using the quantization condition given in Equation (6), we arrive at the following eigenvalues expressions  $(\vartheta_0^\pm, \vartheta_1^\pm, \vartheta_2^\pm, \dots, \vartheta_n^\pm) = -(g \pm \sqrt{P_0}, -1 - g \pm \sqrt{P_0}, -2 - g \pm \sqrt{P_0}, \dots, -n - g \pm \sqrt{P_0})$ . Then, the energy  $E_{nm}$  eigenvalues is given by

$$E_{nm} = Q_0 - Q_1 \frac{[Q_2 - (n + g)^2]^2}{(n + g)^2}, \tag{7}$$

where  $Q_0 = \hbar^2 \delta^2 \tilde{m} / 2\mu + p$ ,  $Q_1 = \hbar^2 \delta^2 / 8\mu$  and  $Q_2 = 2\mu pq / \hbar^2 \delta + \mu^2 \omega_c^2 / \hbar^2 \delta^2 - \tilde{m}$ . Then, the wave function  $R_{nm}(t)$  is given by  $R_{nm}(t) = (-1)^n N_{nm} \Gamma(2\vartheta + 1 + n) / \Gamma(2\vartheta + 1) t^\vartheta (1 - t)^\vartheta {}_2F_1(-n, 2(\vartheta + g) + n; 2\vartheta + 1; t)$ , where  $\Gamma(\cdot)$  is the gamma function and  ${}_2F_1(\cdot)$  is the hypergeometric function.

### 3. Magnetotransport and Thermal Properties of Varshni–Shukla Potential (V–SP)

In order to evaluate the thermal, magnetic and transport properties of the Varshni–Shukla potential, it is required that the energy level accessible be summed; on doing this, the partition function is obtained. Virtually all the aforementioned properties depend on the partition. This would mean that on successful evaluation of the partition function, the magnetotransport and thermal properties are derived. From Equation (7), the partition function  $Z(\beta)$  of the Varshni–Shukla potential for a finite temperature  $T$ , can be derived by utilizing the Boltzmann statistics as  $Z(\beta) = \sum_n e^{-\beta E_n}$ , where  $n = 0, 1, 2 \dots n_{max}$  is the vibrational quantum number and  $\beta = 1/k_B T$  with  $k_B$  is the Boltzmann constant [37–39]. Here,  $n_{max}$  signifies the upper bound vibration quantum number and can be obtained by setting  $\partial E_n / \partial n = 0$ , which is given by  $n_{max} = -g \pm \sqrt{Q_2}$ . On conversion of the summation to an integral and using the transformation  $y = Q_2 / (n + Q_3) - (n + Q_3)$ , the partition function of the Varshni–Shukla potential in magnetic and AB fields with topological defects is obtained as follows:

$$Z(\beta) = \frac{\sqrt{\pi}}{2} e^{-\beta Q_0} \left[ \frac{\text{Erfi}[\sqrt{Q_1} y_1 \sqrt{\beta}] - \text{Erfi}[\sqrt{Q_1} \beta y_2]}{2\sqrt{Q_1} \beta} - \frac{e^{-4Q_1 Q_2} \text{Erfi}[\sqrt{Q_1} \beta (4Q_2 + y_1^2)] - \text{Erfi}[\sqrt{Q_1} \beta (4Q_2 + y_2^2)]}{2\sqrt{Q_1} \beta} \right], \tag{8}$$

where  $y_1 = Q_2 / Q_3 - Q_3$  and  $y_2 = Q_2 / (n_{max} + Q_3) - (n_{max} + Q_3)$ . This expression represents the classical partition function. The reason is that the PF does not contain quantum corrections [37]. The PF is graphically analyzed in Figure 1. In these plots, the partition function (PF) is plotted as a function of the magnetic field, AB field, and topological defect, respectively. It is observed that in Figure 1a, the PF increases as the magnetic field increases for various values of the temperature. When the PF is plotted against the AB field as shown in Figure 1b, it is noticed to move slowly; thereafter, a sharp increase is noticed for different values of the temperature of  $50 \text{ k}^{-1}$  (green curve),  $100 \text{ k}^{-1}$  (blue curve) and  $150 \text{ k}^{-1}$  (red curve). In Figure 1c, we notice that the plot of PF against topological defect decreases and later converges at a point.

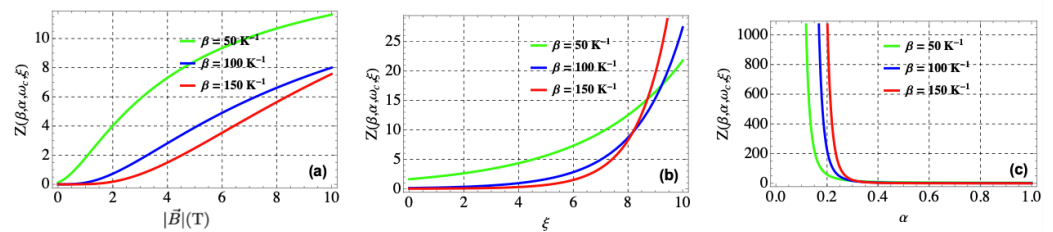


**Figure 1.** (a) Plot of partition function  $Z(\beta)$  as a function of magnetic field  $|\vec{B}|$  (T) with different values of  $\beta$  and fixed values of  $\alpha = 0.4$  and  $\xi = 6$ . (b) Plot of  $Z(\beta)$  as a function of  $\xi$  for different values of  $\beta$  and fixed values of  $|\vec{B}| = 4T$  and  $\alpha = 0.4$ . (c)  $Z(\beta)$  plot as a function of  $\alpha$  for different values of  $\beta$  and fixed values of  $|\vec{B}| = 6T$  and  $\xi = 6$ . For all three plots,  $\beta = 50 \text{ k}^{-1}$  (green curve),  $100 \text{ k}^{-1}$  (blue curve) and  $150 \text{ k}^{-1}$  (red curve) and the maximum vibrational quantum  $n_{max}$  is fixed at  $n_{max} = 100$ ,  $p = q = 0.15$  and  $\delta = 0.005$ .

In what follows, all thermodynamic and magnetic properties of the Varshni–Shukla potential in the presence of the AB and magnetic fields with topological defect, such as the free energy, mean energy, the entropy, specific heat, magnetization, magnetic susceptibility and the persistent current, can be obtained from the partition function  $Z(\beta)$ .

### 3.1. Free Energy

In this section, we discuss the free energy  $F(\beta) = -\ln Z(\beta) / \beta$  [40] of the system. The free energy as a function of the magnetic field, AB field, and topological defect are shown in Figure 2. In Figure 2a, it is observed that the free energy decreases as the magnetic field increases for different values of the temperature. In the plot of the free energy against the AB field (Figure 2b), it is observed that as the AB field decreases, the free energy decreases, for different values of the temperature. In Figure 2c, the free energy increases as the topological defect increases, which exhibits saturation. In line with the stability criterion, which suggests that a system is stable if its Helmholtz energy is minute [41,42], a close observation of the numerical values on the scale of our plots in Figure 2 shows that the free energy satisfies this criterion.

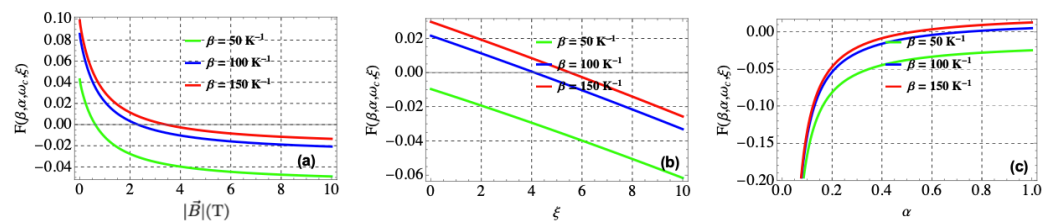


**Figure 2.** (a) Free energy  $F(\beta)$  as a function of: (a)  $|\vec{B}|$  (T) for different values of  $\beta$ ; (b)  $\xi$  for same different values of  $\beta$ ; (c)  $\alpha$  for different values of  $\beta$ . For all three plots,  $\beta = 50 \text{ k}^{-1}$  (green curve),  $100 \text{ k}^{-1}$  (blue curve) and  $150 \text{ k}^{-1}$  (red curve); all other parameters are the same as in Figure 1.

### 3.2. Entropy

In this section, we study the entropy  $S(\beta) = \ln Z(\beta) - \beta \frac{\partial \ln Z}{\partial \beta}$  [38] of the Varshni–Shukla potential. In Figure 3, the entropy is plotted as a function of the magnetic field (a), AB field (b), and topological defect (c). In Figure 3a, the entropy is seen to decrease as the magnetic field is increased. A similar trend is noticed in Figure 3c, where the entropy is plotted against the AB field. In the plot of the entropy against the topological defect, an increase in entropy is seen when the topological defect increases. The physical interpretation of this result is that the applied magnetic field makes the magnetic moments of the system able to lower the energy, thereby leading to a lower entropy state where it is magnetized. In this case, the entropy decreases as the magnetic field increases, at least when it is able to give away entropy to its environment. This effect is very important in

magnetic refrigeration because the opposite is also true: a paramagnetic material tends to absorb entropy as the field is decreased.

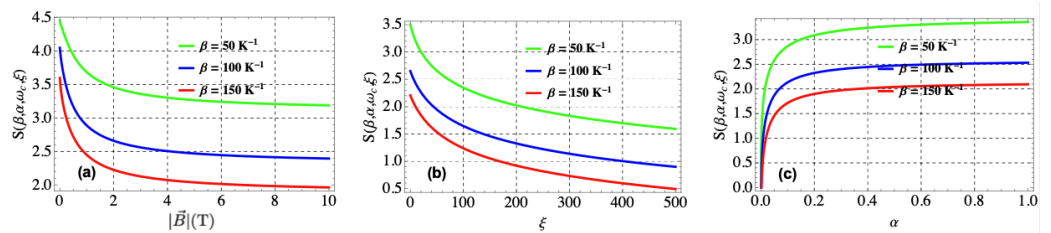


**Figure 3.** Plot of entropy  $S(\beta)$  as a function of  $|\vec{B}|$ (T) (a),  $\xi$  (b) and  $\alpha$  (c) for different values of  $\beta = 50 \text{ k}^{-1}$  (green curve),  $100 \text{ k}^{-1}$  (blue curve) and  $150 \text{ k}^{-1}$  (red curve); all other parameters are the same as in Figure 1.

### 3.3. Internal or Mean Energy

In this section, we analyze the internal energy  $U(\beta) = -\frac{\partial \ln Z(\beta)}{\partial \beta}$  [39] of the system.

In Figure 4, the average energy is plotted as a function of the magnetic field (a), AB field (b) and topological defect (c). In Figure 4a, the average energy decreases as the magnetic field increases for different values of temperature. In Figure 4b, the average energy is seen to have a linear decrease as the AB field increases. We noticed in Figure 4c, that the average energy increases as the topological defect increases.

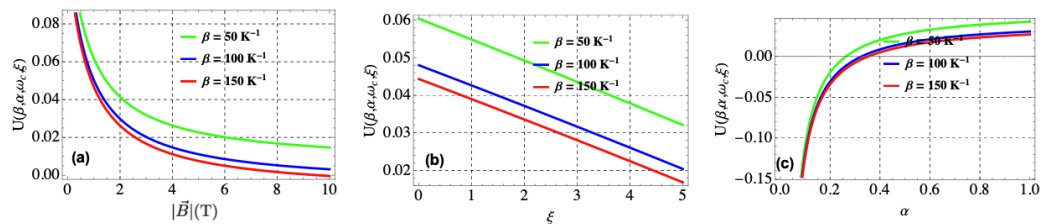


**Figure 4.** Plot of mean energy  $U(\beta)$  as a function of magnetic field  $|\vec{B}|$ (T) (a), AB field  $\xi$  (b) and topological defect  $\alpha$  (c) for different values of  $\beta = 50 \text{ k}^{-1}$  (green curve),  $100 \text{ k}^{-1}$  (blue curve) and  $150 \text{ k}^{-1}$  (red curve); all other parameters are the same as in Figure 1.

### 3.4. Heat Capacity

In this section, we study the heat capacity  $C(\beta) = \beta^2 \frac{\partial^2 \ln Z(\beta)}{\partial \beta^2}$  [39] of the Varshni–Shukla potential. In Figure 5, the specific heat capacity is plotted as a function of the magnetic field, AB field, and topological defect. We observe a similar trend of increase in specific heat capacity as both the magnetic and AB fields are increased. In the plot of the specific heat capacity against the topological defect, a shape increase is noticed followed by a decrease as the topological defect increases. Generally, it is seen that the specific heat capacity exhibits an irregular behavior, which is almost contrary to the fundamental Dulong–Petit law [43]. This anomaly could be attributed to the Schottky anomaly which appears over a small range of temperatures [7,44]. The observation of this Schottky anomaly indicates that there are small numbers of discrete energy levels dominating the behavior of the system, and the spacing between these energy levels can be quantified [7,44,45]. This anomaly may be attributed to the presence of the topological defect.

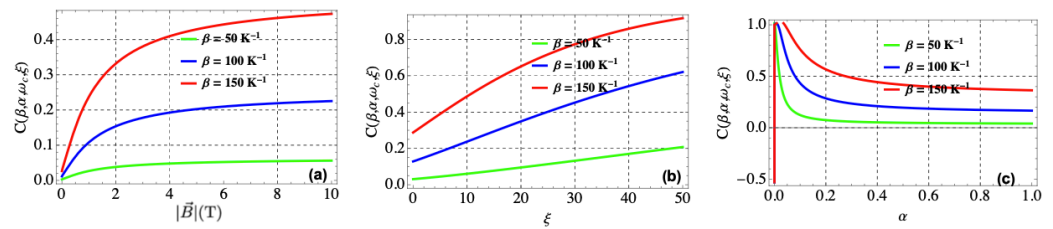


**Figure 5.** Specific heat capacity as a function of (a) magnetic field  $|\vec{B}|(T)$ , (b) AB field  $\xi$  and topological defect  $\alpha$  (c) for different values of  $\beta = 50 \text{ k}^{-1}$  (green curve),  $100 \text{ k}^{-1}$  (blue curve) and  $150 \text{ k}^{-1}$  (red curve); all other parameters are the same as in Figure 1.

3.5. Magnetotransport Properties

In Figure 6, the magnetization  $M(\beta) = \beta^{-1}Z^{-1}(\beta) \frac{\partial Z(\beta)}{\partial \vec{B}}$  is plotted against  $|\vec{B}|$  (a),  $\xi$  (b) and  $\alpha$  (c) for different values of  $\beta$ . In Figure 6a, the magnetization is plotted as a function of the magnetic field, AB field, and topological defect with different values of temperature. Careful observation shows a decrease in magnetization as the magnetic field increases. A similar trend is noticed when the magnetization is plotted as a function of the topological defect. In the plot of the magnetization against the AB field, an increase in magnetization is seen as the AB field is increased. A decreasing magnetization with rising temperature is generally observed here. The reason for this decrease in magnetization with a temperature increase is attributed to the fact that the thermal disorder (kT) increases and opposes the magnetic dipoles of the system to align with the applied magnetic field, which leads to a decreased magnetization.

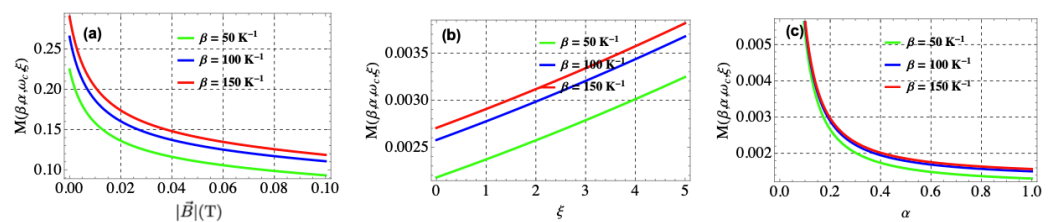


**Figure 6.** Plot of magnetization as function of (a) magnetic field  $|\vec{B}|(T)$ , (b) AB field  $\xi$  and topological defect  $\alpha$  (c) for different values of  $\beta = 50 \text{ k}^{-1}$  (green curve),  $100 \text{ k}^{-1}$  (blue curve) and  $150 \text{ k}^{-1}$  (red curve); all other parameters are the same as in Figure 1.

3.5.1. Magnetic Susceptibility

In Figure 7, the magnetic susceptibility  $\chi(\beta) = \frac{\partial M(\beta)}{\partial \vec{B}}$  [7] is plotted as a function of the magnetic field  $\vec{B}(T)$ , AB field  $\xi$ , and topological defect  $\alpha$  (c) for different values of  $\beta = 50 \text{ k}^{-1}$  (green curve),  $100 \text{ k}^{-1}$  (blue curve) and  $150 \text{ k}^{-1}$  (red curve). A decrease in magnetic susceptibility is observed as the magnetic field increases, which exhibit a diamagnetic behavior as shown in Figure 7a. In Figure 7b, a linear decrease in the magnetic susceptibility is observed as the AB field is increased. In Figure 7c, an increase in the magnetic susceptibility is noticed when the topological defect increases with different values of the temperature.

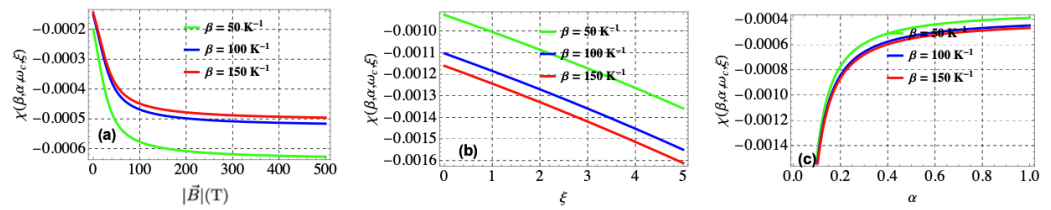


**Figure 7.** Magnetic susceptibility  $\chi(\beta)$  as a function of (a)  $|\vec{B}|(T)$  for different values of  $\beta$  and the same fixed values as in Figure 1a, (b)  $\xi$  for different values of  $\beta$  and the same fixed values as in Figure 1b, (c)  $\alpha$  different values of  $\beta$  and the same fixed values as in Figure 1c. For all three plots,  $\beta = 50 \text{ k}^{-1}$  (green curve),  $100 \text{ k}^{-1}$  (blue curve) and  $150 \text{ k}^{-1}$  (red curve); the maximum vibrational quantum  $n_{max}$  and other parameters are same as in Figure 1.

3.5.2. Persistent Current

In Figure 8, the persistent current  $I(\beta) = -\frac{\partial F(\beta)}{\partial \phi_{AB}}$  [11] is plotted as a function of the magnetic field  $|\vec{B}|$  (a), AB field  $\xi$  (b), and topological defect  $\alpha$  (a) for different values of  $\beta = 50 \text{ k}^{-1}$  (green curve),  $100 \text{ k}^{-1}$  (blue curve) and  $150 \text{ k}^{-1}$  (red curve). In Figure 8a, a linear increase is observed in the persistent current as the magnetic field increases with different values of temperature and this indicates a saturation point. In Figure 8b, a similar trend is noticed in the persistent current as the AB field is increased. In Figure 8c, a decrease is noticed in the persistent current when the topological defect increases for various temperatures. We note here that our understanding of the persistent current of exponential-type potential systems such as the V-SP is far from complete, especially at finite temperatures. We note here again that the persistent current can change its flux’s period and sign (diamagnetic or paramagnetic) as a function of temperature, features that can be attributed to a changing confinement of the system and the presence of the topological defect. This work presents the properties of the persistent current of the V-SP which could be relevant for the interpretation of experiments on persistent currents in such molecular systems.

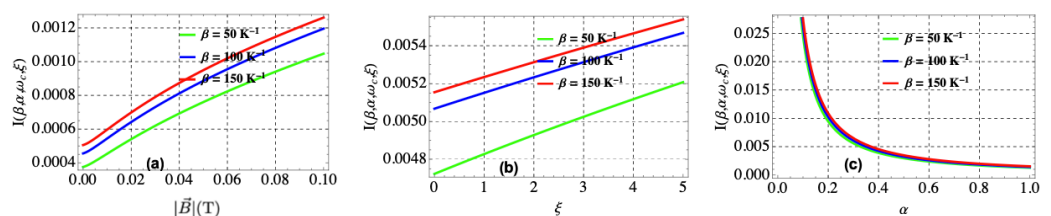


**Figure 8.** Persistent current  $I(\beta)$  as a function of: (a)  $|\vec{B}|(T)$  for different values of  $\beta$  and the same fixed values as in Figure 1a, (b)  $\xi$  for different values of  $\beta$  and the same fixed values as in Figure 1b, (c)  $\alpha$  different values of  $\beta$  and the same fixed values as in Figure 1c. For all three plots,  $\beta = 50 \text{ k}^{-1}$  (green curve),  $100 \text{ k}^{-1}$  (blue curve) and  $150 \text{ k}^{-1}$  (red curve); the maximum vibrational quantum  $n_{max}$  and other parameters are same as in Figure 1.

4. Conclusions

The effects of the magnetic and AB fields and the topological defect (TD) on the magnetic, transport and thermodynamic properties of the Varshni–Shukla potential (V-SP) were analyzed. The AIM was used to derive the energy equation and wave function. The summation of the accessible energy levels was used to obtain the partition function, which was utilized to derive the magnetotransport and thermal properties of the V-SP model. An extensive graphical analysis was carried out to show the effects of the perturbations and topological defect on the thermomagnetic properties. From this study, we find that the defects and external fields contributed to transforming the thermomagnetic and transport properties of the model. Moreover, the thermal and magneto-transport properties were highly sensitive to the magnetic and AB fields and the TD. For instance, in chemical and condensed matter physics, several potential models (such as the exponential-type

potential considered in our study) have been adopted to study the energy spectra and thermodynamics properties of diatomic molecules and GaAs quantum dot, respectively, by several researchers. In view of the foregoing, our results could be applied to study such systems highlighted above, bearing in mind the effects of external fields, which were hitherto not considered.

**Author Contributions:** C.O.E., S.M. and E.P.I. conceived and designed the study, acquired, analyzed and interpreted the data and handled the review; R.E., N.A. and M.A. handled the computational and graphical analysis; M.A., A.N.I. and S.A.A. revised the manuscript for important intellectual content and contributed to the general recommendations and data interpretation. All authors have read and agreed to the published version of the manuscript.

**Funding:** This research was carried out under LRGS Grant LRGS/1/2020/UM/01/5/2 (9012-00009) Fault-tolerant Photonic Quantum States for Quantum Key Distribution provided by the Ministry of Higher Education of Malaysia (MOHE).

**Data Availability Statement:** The datasets used and/or analyzed during the current study are available from the corresponding author on reasonable request.

**Conflicts of Interest:** The authors declare no conflict of interest.

## References

1. Marques, G.D.A.; Bezerra, V.B. Hydrogen atom in the gravitational fields of topological defects. *Phys. Rev. D* **2002**, *66*, 105011. [[CrossRef](#)]
2. Bakke, K.; Furtado, C. On the interaction of the Dirac oscillator with the Aharonov–Casher system in topological defect backgrounds. *Ann. Phys.* **2013**, *336*, 489–504. [[CrossRef](#)]
3. Bakke, K.; Ribeiro, L.R.; Furtado, C.; Nascimento, J.R. Landau quantization for a neutral particle in the presence of topological defects. *Phys. Rev. D* **2009**, *79*, 024008. [[CrossRef](#)]
4. Carvalho, J.; Furtado, C.; Moraes, F. Dirac oscillator interacting with a topological defect. *Phys. Rev. A* **2011**, *84*, 032109. [[CrossRef](#)]
5. Marques, G.D.A.; Bezerra, V.B. Non-relativistic quantum systems on topological defects spacetimes. *Class. Quantum Gravity* **2002**, *19*, 985. [[CrossRef](#)]
6. Hassanabadi, H.; Hosseinpour, M. Thermodynamic properties of neutral particle in the presence of topological defects in magnetic cosmic string background. *Eur. Phys. J. C* **2016**, *76*, 1–7. [[CrossRef](#)]
7. Castano-Yepes, J.D.; Amor-Quiroz, D.A.; Ramirez-Gutierrez, C.F.; Gómez, E.A. Impact of a topological defect and Rashba spin-orbit interaction on the thermo-magnetic and optical properties of a 2D semiconductor quantum dot with Gaussian confinement. *Phys. E Low-Dimens. Syst. Nanostruct.* **2019**, *109*, 59–66. [[CrossRef](#)]
8. Hosseinpour, M.; Andrade, F.M.; Silva, E.O.; Hassanabadi, H. Scattering and bound states for the Hulthén potential in a cosmic string background. *Eur. Phys. J. C* **2017**, *77*, 1–6.
9. Nwabuzor, P.; Edet, C.; Ikot, A.N.; Okorie, U.; Ramantswana, M.; Horchani, R.; Abdel-Aty, A.-H.; Rampho, G. Analyzing the Effects of Topological Defect (TD) on the Energy Spectra and Thermal Properties of LiH, TiC and I2 Diatomic Molecules. *Entropy* **2021**, *23*, 1060. [[CrossRef](#)]
10. Edet, C.O.; Ikot, A.N. Effects of Topological Defect on the Energy Spectra and Thermo-magnetic Properties of CO Diatomic Molecule. *J. Low Temp. Phys.* **2021**, *203*, 84–111. [[CrossRef](#)]
11. Aharonov, Y.; Bohm, D. Significance of Electromagnetic Potentials in the Quantum Theory. *Phys. Rev. (Ser. I)* **1959**, *115*, 485–491. [[CrossRef](#)]
12. Edet, C.; Nwabuzor, P.; Ettah, E.; Duque, C.; Ali, N.; Ikot, A.; Mahmoud, S.; Asjad, M. Magneto-transport and thermal properties of the Yukawa potential in cosmic string space-time. *Results Phys.* **2022**, *39*, 105749. [[CrossRef](#)]
13. Edet, C.O.; Amadi, P.O.; Ettah, E.B.; Ali, N.; Asjad, M.; Ikot, A.N. The magnetocaloric effect, thermo-magnetic and transport properties of LiH diatomic molecule. *Mol. Phys.* **2022**, *120*, e2059025. [[CrossRef](#)]
14. Abu-Shady, M.; Edet, C.; Ikot, A. Non-relativistic quark model under external magnetic and Aharonov–Bohm (AB) fields in the presence of temperature-dependent confined Cornell potential. *Can. J. Phys.* **2021**, *99*, 1024–1031. [[CrossRef](#)]
15. Khordad, R. Effect of magnetic field on linear and nonlinear optical properties in a parabolic cylindrical quantum dot. *J. Opt.* **2013**, *42*, 83–91. [[CrossRef](#)]
16. Al, E.B.; Kasapoglu, E.; Sari, H.; Sökmen, I. Zeeman splitting, Zeeman transitions and optical absorption of an electron confined in spherical quantum dots under the magnetic field. *Philos. Mag.* **2020**, *101*, 117–128. [[CrossRef](#)]
17. Ikhdair, S.M.; Falaye, B.J.; Hamzavi, M. Nonrelativistic molecular models under external magnetic and AB flux fields. *Ann. Phys.* **2015**, *353*, 282–298. [[CrossRef](#)]
18. Ikot, A.N.; Edet, C.; Amadi, P.O.; Okorie, U.S.; Rampho, G.J.; Abdullah, H.Y. Thermodynamic properties of Aharonov–Bohm (AB) and magnetic fields with screened Kratzer potential. *Eur. Phys. J. D* **2020**, *74*, 1–13. [[CrossRef](#)]

19. M'Zerd, S.; El Haouari, M.; Talbi, A.; Feddi, E.; Mora-Ramos, M. Impact of electron-LO-phonon correction and donor impurity localization on the linear and nonlinear optical properties in spherical core/shell semiconductor quantum dots. *J. Alloys Compd.* **2018**, *753*, 68–78. [[CrossRef](#)]
20. Edet, C.O.; Ettah, E.B.; Aljunid, S.A.; Endut, R.; Ali, N.; Ikot, A.N.; Asjad, M. Global Quantum Information-Theoretic Measures in the Presence of Magnetic and Aharonov-Bohm (AB) Fields. *Symmetry* **2022**, *14*, 976. [[CrossRef](#)]
21. Edet, C.O.; Lima, F.C.E.; Almeida, C.A.S.; Ali, N.; Asjad, M. Quantum Information of the Aharonov–Bohm Ring with Yukawa Interaction in the Presence of Disclination. *Entropy* **2022**, *24*, 1059. [[CrossRef](#)]
22. Tavares, C.; Oliveira, S.; Fernandes, V.; Postnikov, A.; Vasilevskiy, M.I. Quantum simulation of the ground-state Stark effect in small molecules: A case study using IBM Q. *Soft Comput.* **2021**, *25*, 6807–6830. [[CrossRef](#)]
23. Rastegar-Sedehi, H.R. Magnetocaloric effect in Rashba spin–orbit coupling and Zeeman splitting of a narrow nanowire quantum dot. *Eur. Phys. J. Plus* **2021**, *136*, 1–8. [[CrossRef](#)]
24. Rampho, G.J.; Ikot, A.N.; Edet, C.O.; Okorie, U.S. Energy spectra and thermal properties of diatomic molecules in the presence of magnetic and AB fields with improved Kratzer potential. *Mol. Phys.* **2020**, *119*, e1821922. [[CrossRef](#)]
25. Edet, C.O.; Amadi, P.O.; Onyeaju, M.C.; Okorie, U.S.; Sever, R.; Rampho, G.J.; Abdullah, H.Y.; Salih, I.H.; Ikot, A.N. Thermal Properties and Magnetic Susceptibility of Hellmann Potential in Aharonov–Bohm (AB) Flux and Magnetic Fields at Zero and Finite Temperatures. *J. Low Temp. Phys.* **2020**, *202*, 83–105. [[CrossRef](#)]
26. Karayer, H. Study of the radial Schrödinger equation with external magnetic and AB flux fields by the extended Nikiforov–Uvarov method. *Eur. Phys. J. Plus* **2020**, *135*, 1–10. [[CrossRef](#)]
27. Edet, C.O.; Ikot, A.N. Shannon information entropy in the presence of magnetic and Aharonov–Bohm (AB) fields. *Eur. Phys. J. Plus* **2021**, *136*, 1–11. [[CrossRef](#)]
28. Oluwadare, O.J.; Oyewumi, K.J. Scattering state solutions of the Duffin-Kemmer-Petiau equation with the Varshni potential model. *Eur. Phys. J. A* **2017**, *53*, 1–6. [[CrossRef](#)]
29. Oluwadare, O.J.; Oyewumi, K.J. The semi-relativistic scattering states of the two-body spinless Salpeter equation with the Varshni potential model. *Eur. Phys. J. Plus* **2017**, *132*, 277. [[CrossRef](#)]
30. Oluwadare, O.; Oyewumi, K.J. Scattering states solutions of Klein–Gordon equation with three physically solvable potential models. *Chin. J. Phys.* **2017**, *55*, 2422–2435. [[CrossRef](#)]
31. Varshni, Y.P. Comparative study of potential energy functions for diatomic molecules. *Rev. Mod. Phys.* **1957**, *29*, 664. [[CrossRef](#)]
32. Inyang, E.P.; Inyang, E.P.; William, E.S.; Ibekwe, E.E. Study on the applicability of Varshni potential to predict the mass-spectra of the Quark-antiquark systems in a non-relativistic framework. *Jordan J. Phys.* **2021**, *14*, 337–345.
33. Bayrak, O.; Boztosun, I. Bound state solutions of the Hulthén potential by using the asymptotic iteration method. *Phys. Scr.* **2007**, *76*, 92. [[CrossRef](#)]
34. Greene, R.L.; Aldrich, C. Variational wave functions for a screened Coulomb potential. *Phys. Rev. A* **1976**, *14*, 2363–2366. [[CrossRef](#)]
35. Ciftci, H.; Hall, R.; Saad, N. Asymptotic iteration method for eigenvalue problems. *J. Phys. A Math. Gen.* **2003**, *36*, 11807–11816. [[CrossRef](#)]
36. Falaye, B.J. Any l-state solutions of the Eckart potential via asymptotic iteration method. *Cent. Eur. J. Phys.* **2012**, *10*, 960–965. [[CrossRef](#)]
37. Jia, C.-S.; Wang, C.-W.; Zhang, L.-H.; Peng, X.-L.; Zeng, R.; You, X.-T. Partition function of improved Tietz oscillators. *Chem. Phys. Lett.* **2017**, *676*, 150–153. [[CrossRef](#)]
38. Jia, C.-S.; Zhang, L.-H.; Peng, X.-L.; Luo, J.-X.; Zhao, Y.-L.; Liu, J.-Y.; Guo, J.-J.; Tang, L.-D. Prediction of entropy and Gibbs free energy for nitrogen. *Chem. Eng. Sci.* **2019**, *202*, 70–74. [[CrossRef](#)]
39. Wang, J.; Jia, C.-S.; Li, C.-J.; Peng, X.-L.; Zhang, L.-H.; Liu, J.-Y. Thermodynamic Properties for Carbon Dioxide. *ACS Omega* **2019**, *4*, 19193–19198. [[CrossRef](#)]
40. Edet, C.O.; Okorie, U.S.; Osobonye, G.; Ikot, A.N.; Rampho, G.J.; Sever, R. Thermal properties of Deng–Fan–Eckart potential model using Poisson summation approach. *J. Math. Chem.* **2020**, *58*, 989–1013. [[CrossRef](#)]
41. Kria, M.; Feddi, K.; Aghoutane, N.; El-Yadri, M.; Pérez, L.M.; Laroze, D.; Dujardin, F.; Feddi, E. Thermodynamic properties of SnO<sub>2</sub>/GaAs core/shell nanofiber. *Phys. A Stat. Mech. Its Appl.* **2020**, *560*, 125104. [[CrossRef](#)]
42. Lakaal, K.; Kria, M.; El Hamdaoui, J.; Varsha; Prasad, V.; Nautiyal, V.V.; El-Yadri, M.; Pérez, L.; Laroze, D.; Feddi, E. Polaronic corrections on magnetization and thermodynamic properties of electron–electron in 2D systems with Rashba spin–orbit coupling. *J. Magn. Magn. Mater.* **2022**, *551*, 169042. [[CrossRef](#)]
43. Servatkhah, M.; Khordad, R.; Firoozi, A.; Sedehi, H.R.R.; Mohammadi, A. Low temperature behavior of entropy and specific heat of a three dimensional quantum wire: Shannon and Tsallis entropies. *Eur. Phys. J. B* **2020**, *93*, 1–7. [[CrossRef](#)]
44. Castaño-Yepes, J.; Ramirez-Gutierrez, C.; Correa-Gallego, H.; Gómez, E.A. A comparative study on heat capacity, magnetization and magnetic susceptibility for a GaAs quantum dot with asymmetric confinement. *Phys. E Low-Dimens. Syst. Nanostruct.* **2018**, *103*, 464–470. [[CrossRef](#)]
45. Adhikari, R.B.; Shen, P.; Kunwar, D.L.; Jeon, I.; Maple, M.B.; Dzero, M.; Almasan, C.C. Magnetic field dependence of the Schottky anomaly in filled skutterudites Pr<sub>1-x</sub>Eu<sub>x</sub>Pt<sub>4</sub>Ge<sub>12</sub>. *Phys. Rev. B* **2019**, *100*, 174509. [[CrossRef](#)]